YHO, an air-stable ionic hydride

Nicolas Zapp†, Henry Auer†, Holger Kohlmann†

† Inorganic Chemistry, Leipzig University, Germany

Supplementary information to the publication in Inorganic Chemistry, 2019

Content

X-Ray Diffraction 2

Differential Scanning Calorimetry (DSC) 9

In situ X-ray Powder Diffraction 10

Crystal Structure Discussion and Bärnighausen Tree 11

Anionic Ordering Scheme 13

Density Functional Theory (DFT) Calculations 14

- Reaction Enthalpies 14
- Density of States 15

References 16

X-Ray Diffraction

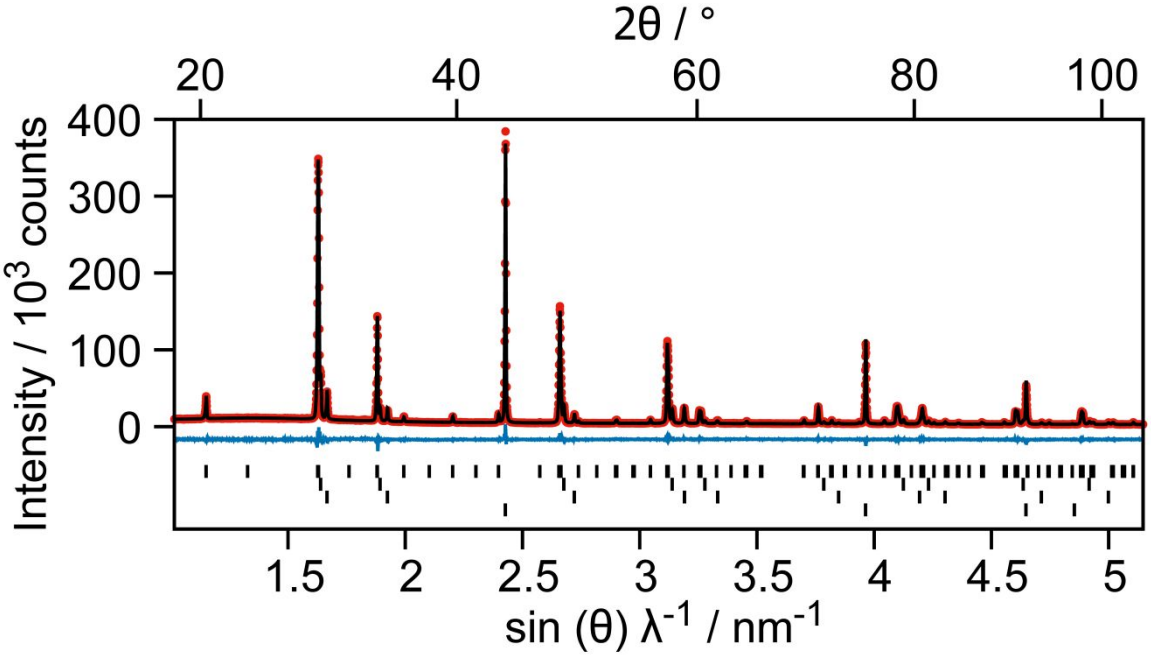

Figure S1 Rietveld refinement of the crystal structure of YDO based on powder X-ray diffraction data at 296(2) K (Stoe STADI-P, λ: $CuK_{\alpha1}$; R_{wp} = 5.0%, *GooF* = 4.4; Bragg markers denote from top to bottom: YDO *Pnma* (82.0(2) wt.-%, R_{Bragg} = 2.2%, *a* = 7.52953(6) Å, *b* = 3.75264(3) Å, *c* = 5.31805(5) Å), YDO $Fm\bar{3}m$ (11.66(10) wt.-%, *a* = 5.28276(5) Å), YD_2 $Fm\bar{3}m$ (6.33(6) wt.-%, *a* = 5.19586(6) Å), C (diamond, added as internal standard and in order to reduce X-ray absorption) $Fd\bar{3}m$) . Red: measurement, black: calculated, blue: difference.

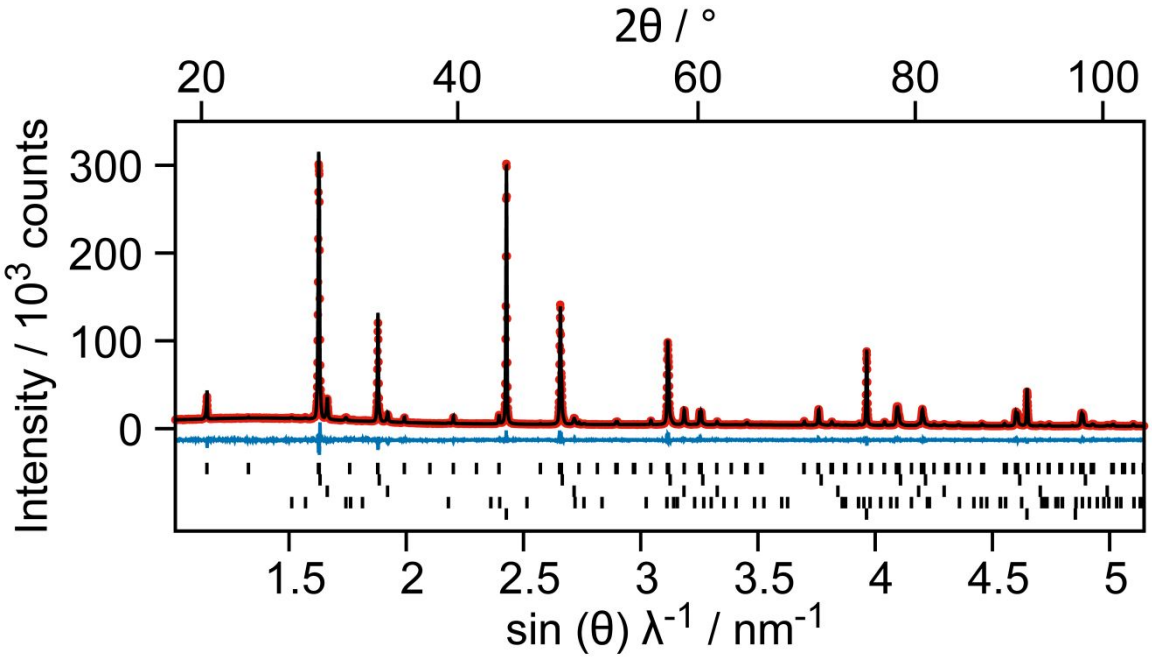

Figure S2 Rietveld refinement of the crystal structure of YHO based on powder X-ray diffraction data at 296(2) K (Stoe STADI-P, λ: $CuK_{\alpha1}$; R_{wp} = 4.4%, *GooF* = 3.7; Bragg markers denote from top to bottom: YHO *Pnma* (83.3(5) wt.-%, R_{Bragg} = 2.2%, *a* = 7.53390(5) Å, *b* = 3.75593(2) Å, *c* = 5.32335(4) Å), YHO $Fm\bar{3}m$ (8.4(5) wt.-%, *a* = 5.3037(6) Å), YH_2 $Fm\bar{3}m$ (6.99(7) wt.-%, *a* = 5.20576(9) Å), YH_3 $P\bar{3}c1$ (1.26(4) wt.-%, *a* = 6.3666(8) Å, *c* = 6.614(1) Å), C (diamond, added as internal standard and in order to reduce X-ray absorption) $Fd\bar{3}m$). Red: measurement, black: calculated, blue: difference.

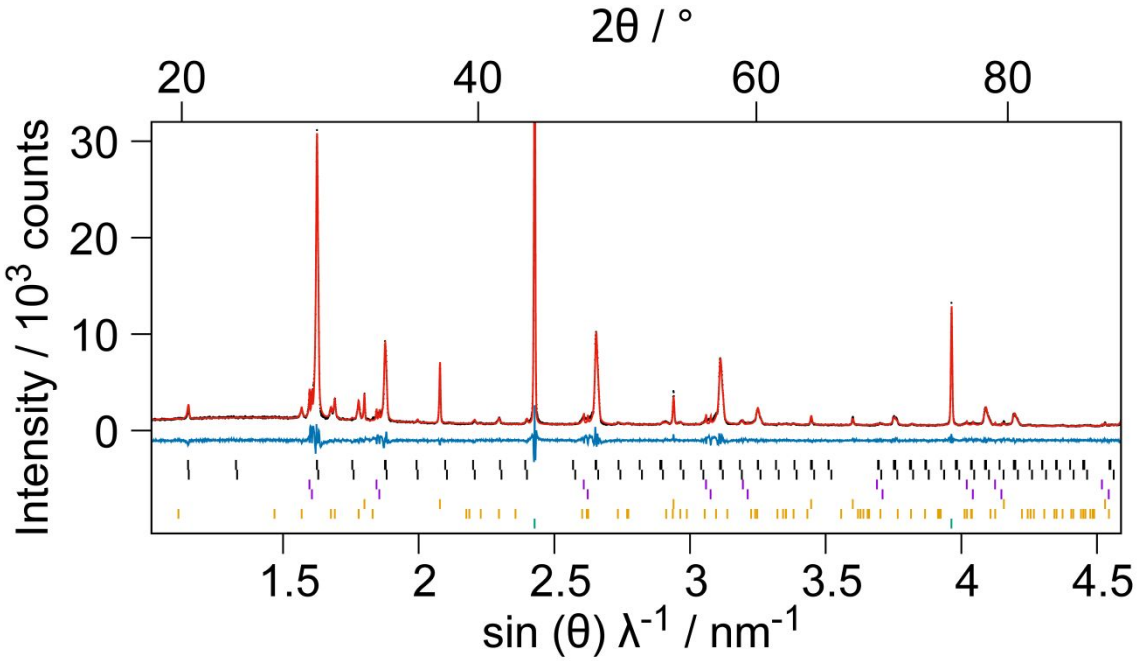

Figure S3 Rietveld refinement of the crystal structure of YHO obtained from Y_2O_3 and CaH_2 (Stoe STADI-P, *λ*: $CuK_{\alpha1}$; R_{wp} = 8.4%, *GooF* = 2.9; Bragg markers denote from top to bottom: YHO *Pnma* (53.3(5) wt.-%, R_{Bragg} = 1.5%, *a* = 7.5360(12) Å, *b* = 3.7698(7) Å, *c* = 5.3223(5) Å), Y_2O_3 $Ia\bar{3}$ (9.7(3) wt.-%, *a* = 10.6242(5) Å), $(Ca,Y)H_x$ $Fm\bar{3}m$ (fraction 1; 3(1) wt.-%, *a* = 5.42 Å), $(Ca,Y)H_x$ $Fm\bar{3}m$ (fraction 2; 3(1) wt.-%, *a* = 5.39 Å), CaO $Fm\bar{3}m$ (15.45(17) wt.-%, *a* = 4.81026(6) Å), CaH_2 *Pnma* (15.6(3) wt.-%, *a* = 5.9632(7) Å, *b* = 3.6056(4) Å, *c* = 6.8083(7) Å), C (diamond, added as internal standard and in order to reduce X-ray absorption) $Fd\bar{3}m$). Red: measurement, black: calculated, blue: difference. Broad reflections left to those of YHO were attributed to two fractions of a solid solution series $(Ca,Y)H_x$, which were constrained by lattice parameters in the refinement.

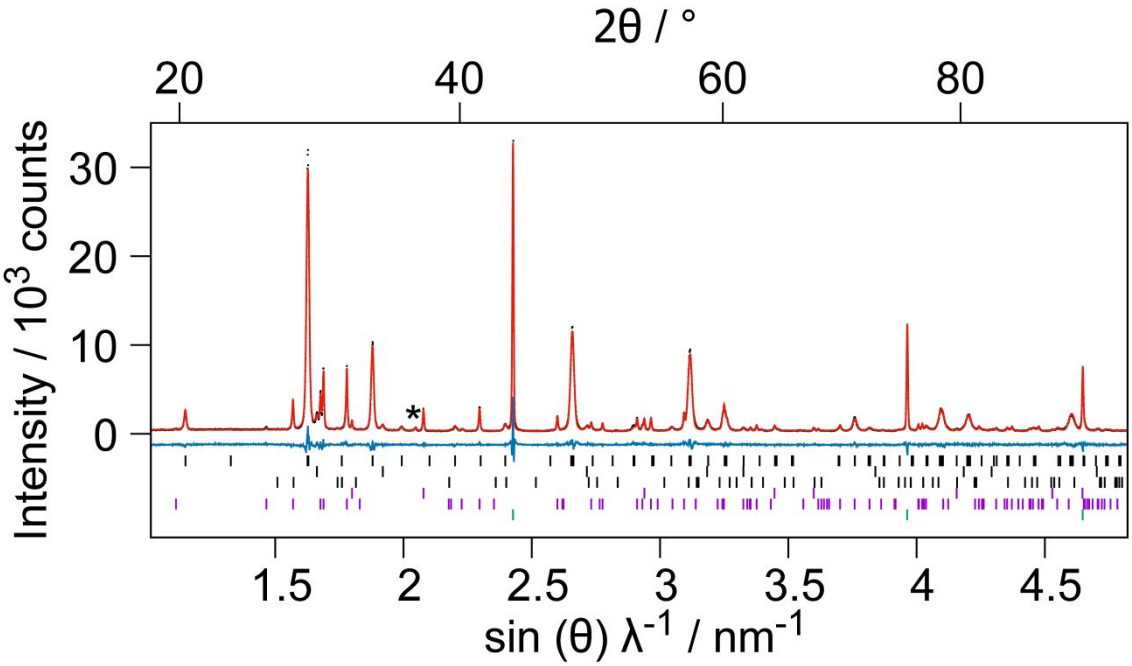

Figure S4 Rietveld refinement of the crystal structure of YHO obtained from YH_3 and CaO (Stoe STADI-P, λ: $CuK_{\alpha 1}$; R_{wp} = 7.4%, *GooF* = 2.3; Bragg markers denote from top to bottom: YHO *Pnma* (61.3(3) wt.-%, R_{Bragg} = 2.0%, *a* = 7.5344(4) Å, *b* = 3.7548(2) Å, *c* = 5.3192(3) Å), YH_2 $Fm\bar{3}m$ (2.66(4) wt.-%, *a* = 5.2079(3) Å), YH_3 $P\bar{3}c1$ (0.52(5) wt.-%, *a* = 6.362(5) Å, *c* = 6.63(1) Å), CaO $Fm\bar{3}m$ (6.34(11) wt.-%, *a* = 4.8110(1) Å), CaH_2 *Pnma* (29.2(2) wt.-%, *a* = 5.9636(1) Å, *b* = 3.60144(7) Å, *c* = 6.8216(1) Å), C (diamond, added as internal standard and in order to reduce X-ray absorption) $Fd\bar{3}m$). Red: measurement, black: calculated, blue: difference. The asterisk marks an unidentified reflection.

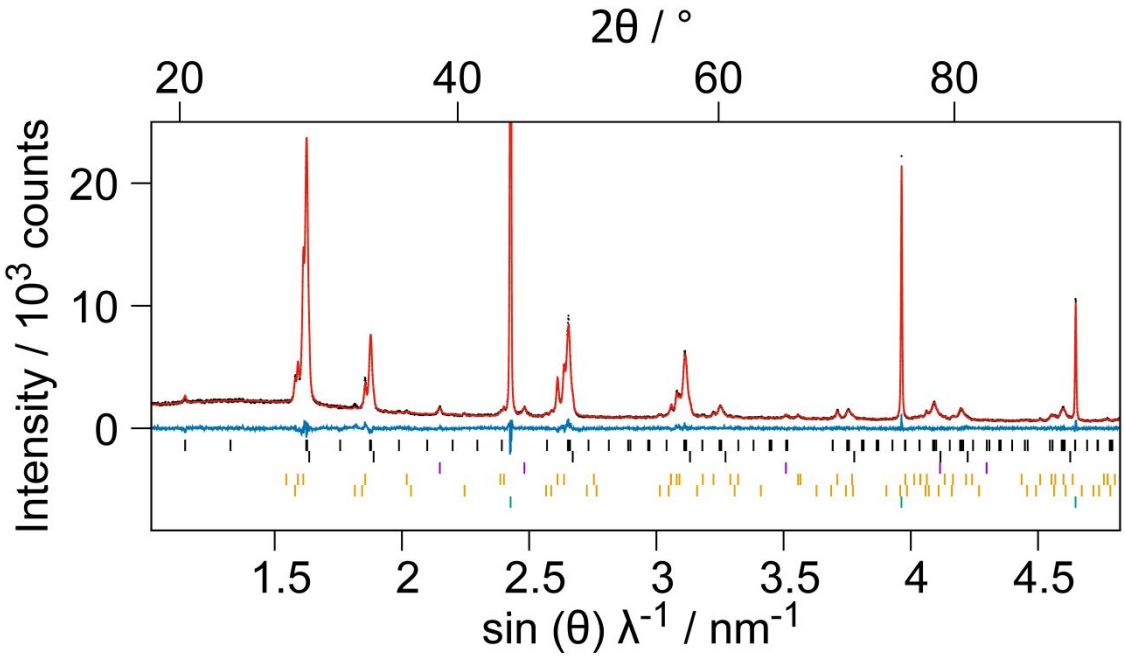

Figure S5 Rietveld refinement of the crystal structure of YHO obtained from YOF and LiH (Stoe STADI-P, *λ*: $CuK_{\alpha 1}$; R_{wp} = 3.9%, *GooF* = 1.6; Bragg markers denote from top to bottom: YHO *Pnma* (48.8(4) wt.-%, R_{Bragg} = 1.4%, *a* = 7.5381(5) Å, *b* = 3.7572(4) Å, *c* = 5.3326(4) Å), YHO $Fm\bar{3}m$ (3.5(3) wt.-%, 5.2930(3) Å), LiF $Fm\bar{3}m$ (15.5(4) wt.-%, *a* = 4.0290(3) Å), YOF $R\bar{3}m$ (30.2(3) wt.-%, *a* = 3.79104(8) Å, *c* = 18.8476(6) Å), YOF *P*4/*nmm* (2.20(6) wt.-%, *a* = 3.8953(4) Å, *c* = 5.423(1) Å), C (diamond, added as internal standard and in order to reduce X-ray absorption) $Fd\bar{3}m$). Red: measurement, black: calculated, blue: difference.

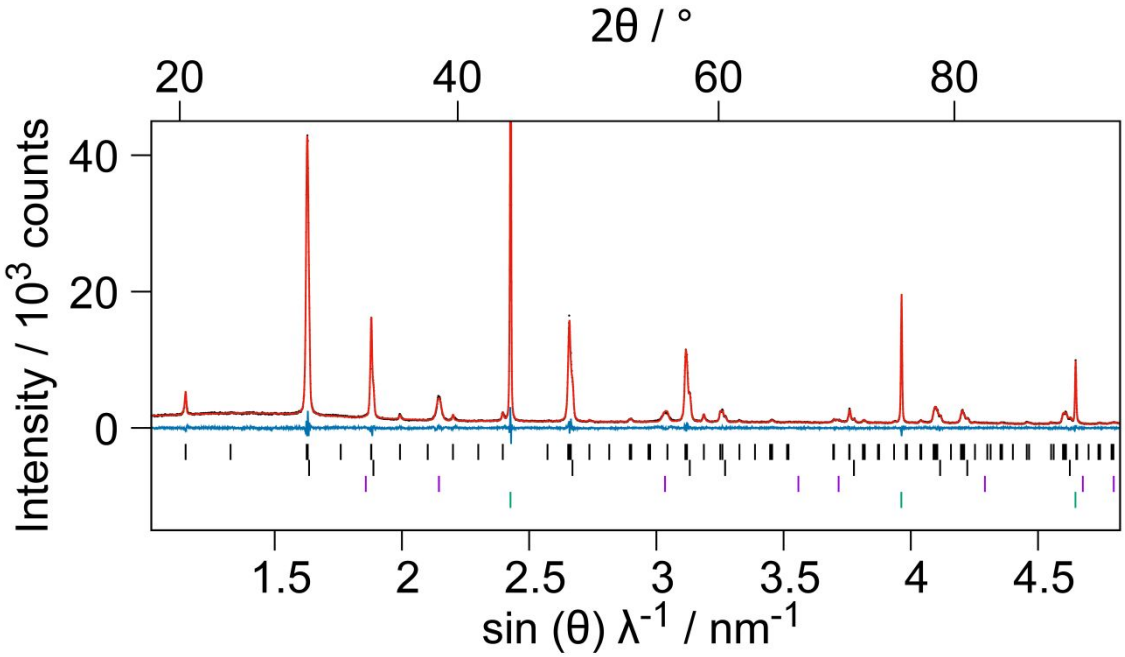

Figure S6 Rietveld refinement of the crystal structure of YHO obtained from YOF and NaH (Stoe STADI-P, λ: $CuK_{\alpha 1}$; R_{wp} = 4.1%, *GooF* = 1.7; Bragg markers denote from top to bottom: YHO *Pnma* (56.1(2) wt.-%, R_{Bragg} = 1.2%, *a* = 7.5358(1) Å, *b* = 3.7534(1) Å, *c* = 5.3211(1) Å), YHO $Fm\bar{3}m$ (13.13(18) wt.-%, *a* = 5.2947(1) Å), NaF $Fm\bar{3}m$ (30.7(4) wt.-%, *a* = 4.6596(1) Å), C (diamond, added as internal standard and in order to reduce X-ray absorption) $Fd\bar{3}m$). Red: measurement, black: calculated, blue: difference.

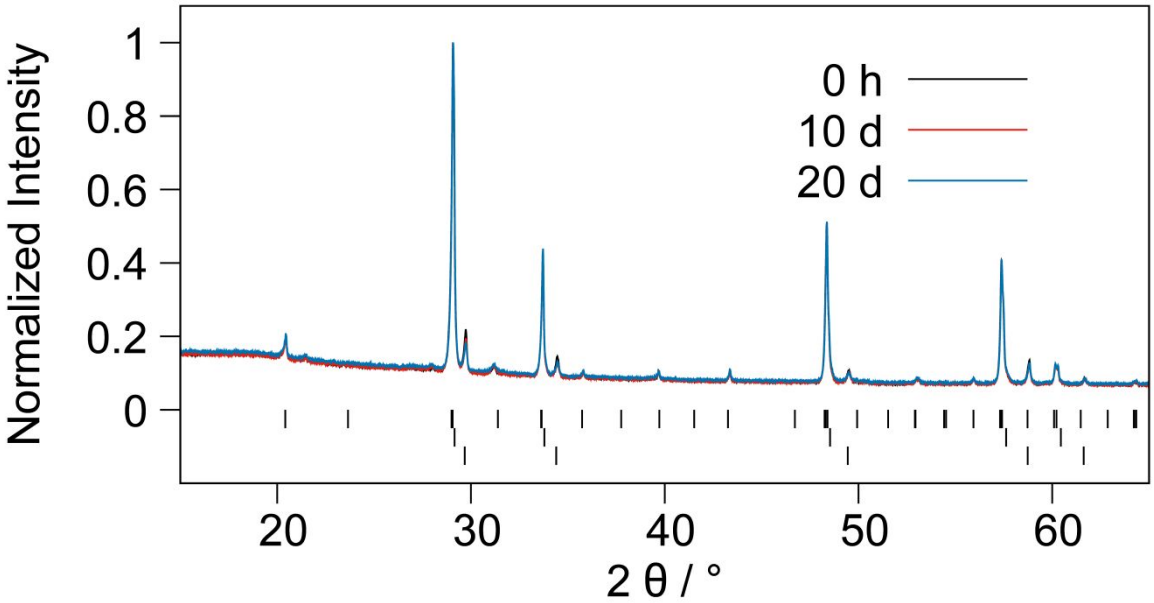

Figure S7 Diffraction patterns of YHO stored in air after 0 h, 10 d and 20 d. Bragg markers denote from top to bottom: YHO *Pnma*, YHO $Fm\bar{3}m$, YH_2 $Fm\bar{3}m$.

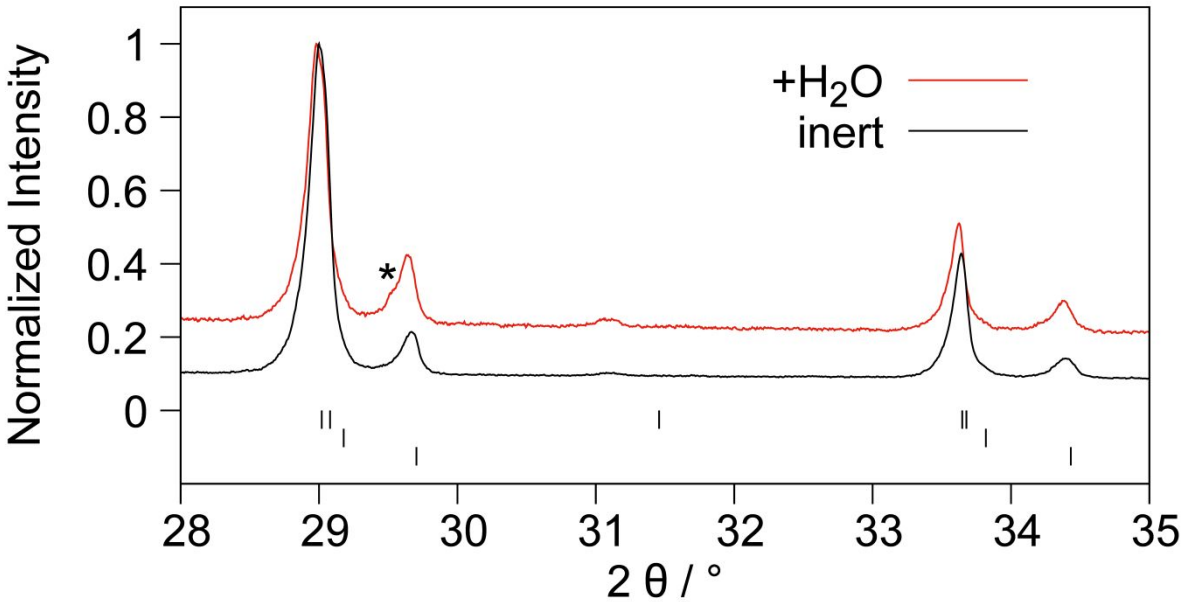

Figure S8 Diffraction patterns of YHO prior and after treatment with liquid H_2O. Bragg markers denote from top to bottom: YHO *Pnma*, YHO $Fm\bar{3}m$, YH_2 $Fm\bar{3}m$. The asterisk marks a further fluorite phase, which is probably O-poor YH_xO_y.[1]

Differential Scanning Calorimetry (DSC)

The reactions of YOF towards LiH and NaH were investigated in a differential scanning calorimeter with attached pressure chamber. The measured DSC plots are shown below.

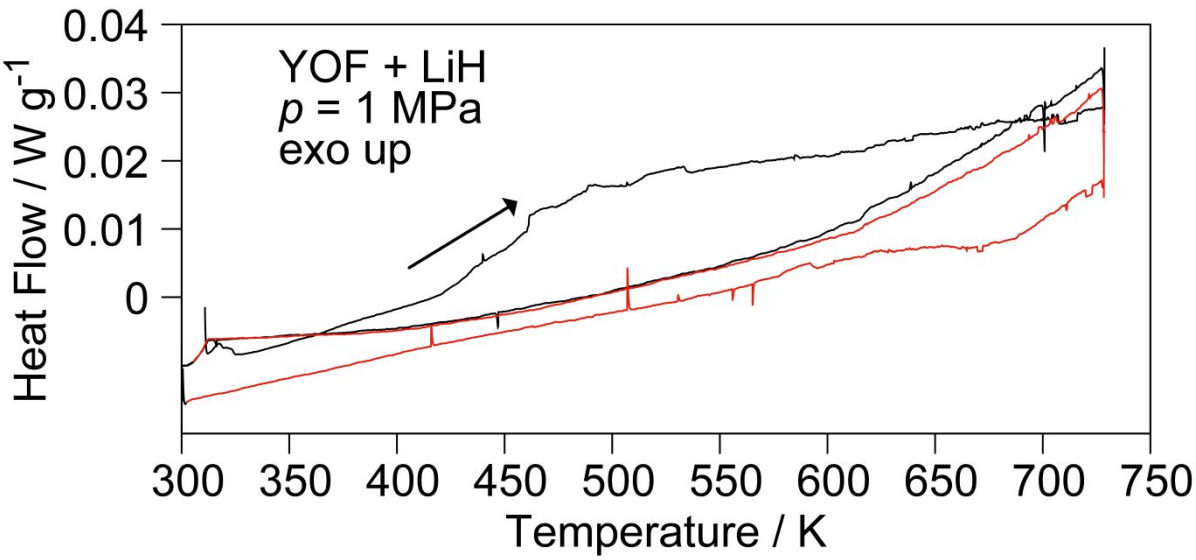

Figure S9 DSC plot of the reaction of YOF and LiH under hydrogen gas pressure. Black: 1st cycle, red: 2nd cycle.

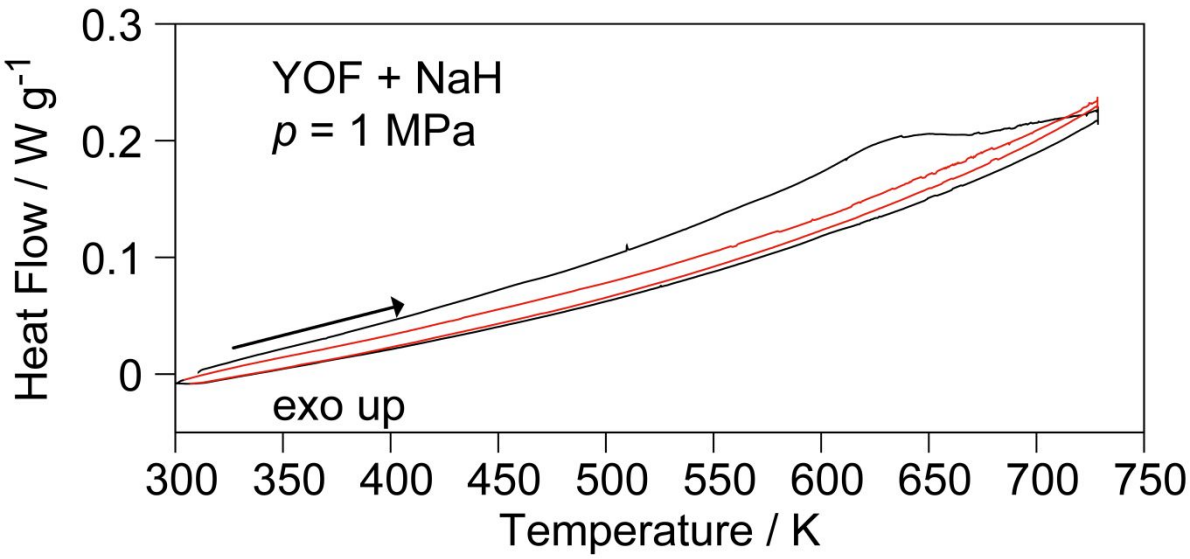

Figure S10 DSC plot of the reaction of YOF and NaH under hydrogen gas pressure. Black: 1st cycle, red: 2nd cycle.

In situ X-ray Powder Diffraction

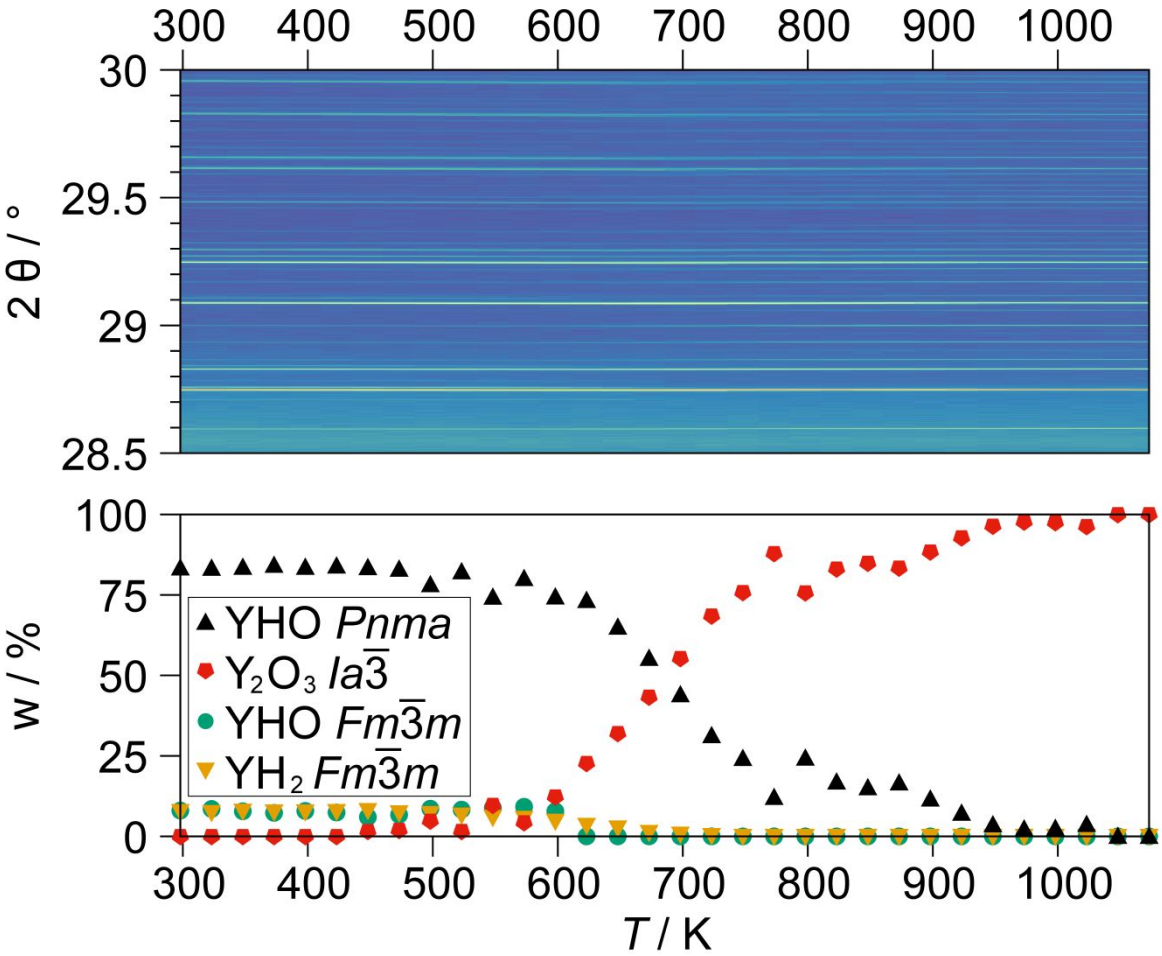

Figure S11 *In situ* X-ray diffraction data and phase contents for the thermal decomposition of YHO in air. Top: diffraction data (λ: $CuK_{\alpha1}$, square root of intensity); bottom: phase contents derived from Rietveld refinement. Error bars are smaller than the displayed symbols.

Crystal Structure Discussion and Bärnighausen Tree

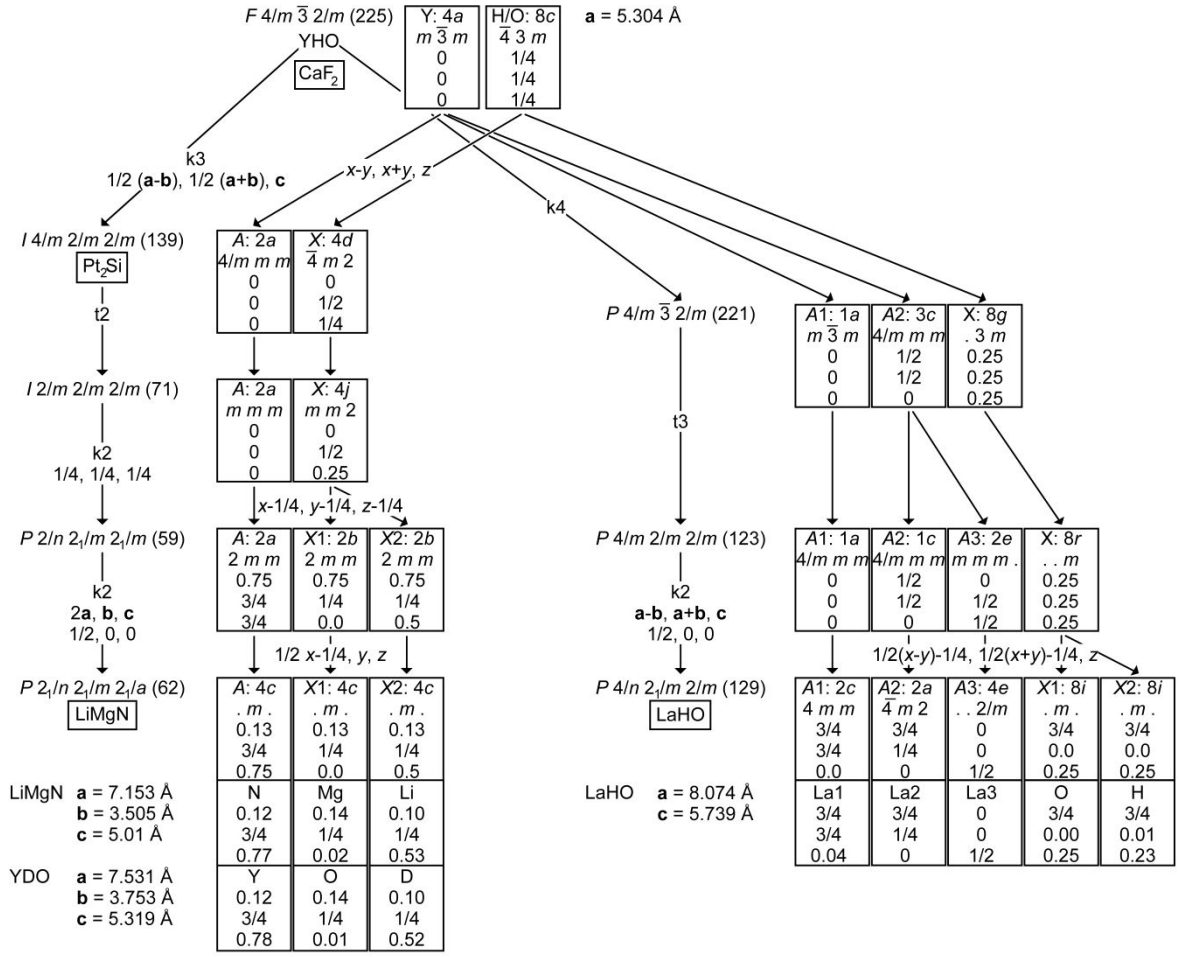

Figure S12 Bärnighausen tree showing the symmetry relationship between the structure types of CaF_2, LaHO and YDO. The relationship between CaF_2 and Pt_2Si was already described in the literature.[2]

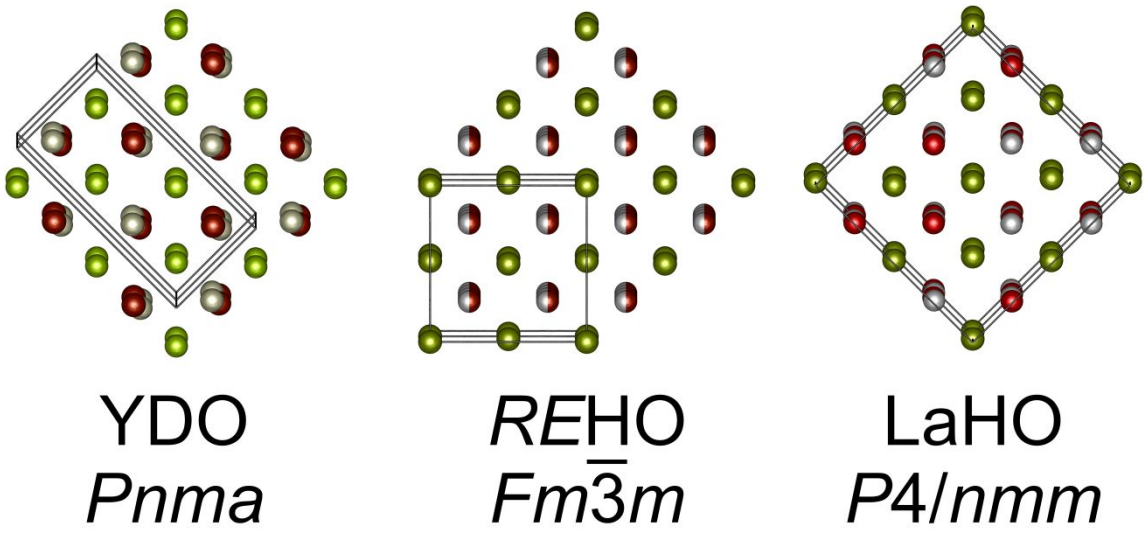

Figure S13 Comparison of the unit cells of anti-LiMgN type YDO, fluorite type *RE*HO and LaHO structure type. Green: *RE* (rare earth), white: H/D, red: O.

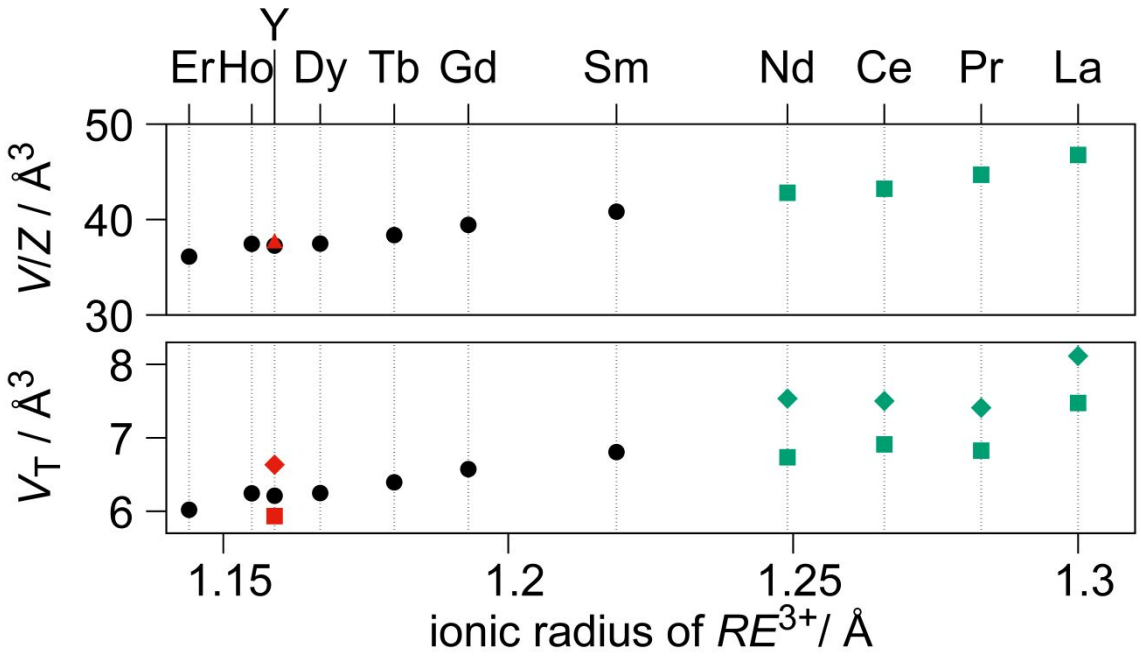

Figure S14 Plot of the normalized unit cell volume (unit cell volume *V* divided by number of formula units *Z*; top) and volume of anion centered coordination polyhedra (V_T; bottom) against radii of eight-fold coordinated RE^{3+} ions.[3] Top ▲: YHO structure determined by powder neutron diffraction, ■: LaHO type structures,[4,5,6] ●: fluorite type structures (YHO determined by powder neutron diffraction; values of Sm – Er taken from the literature).[7] Bottom ■: O^{2-} polyhedra, ◆: H^- polyhedra.

Anionic Ordering Scheme

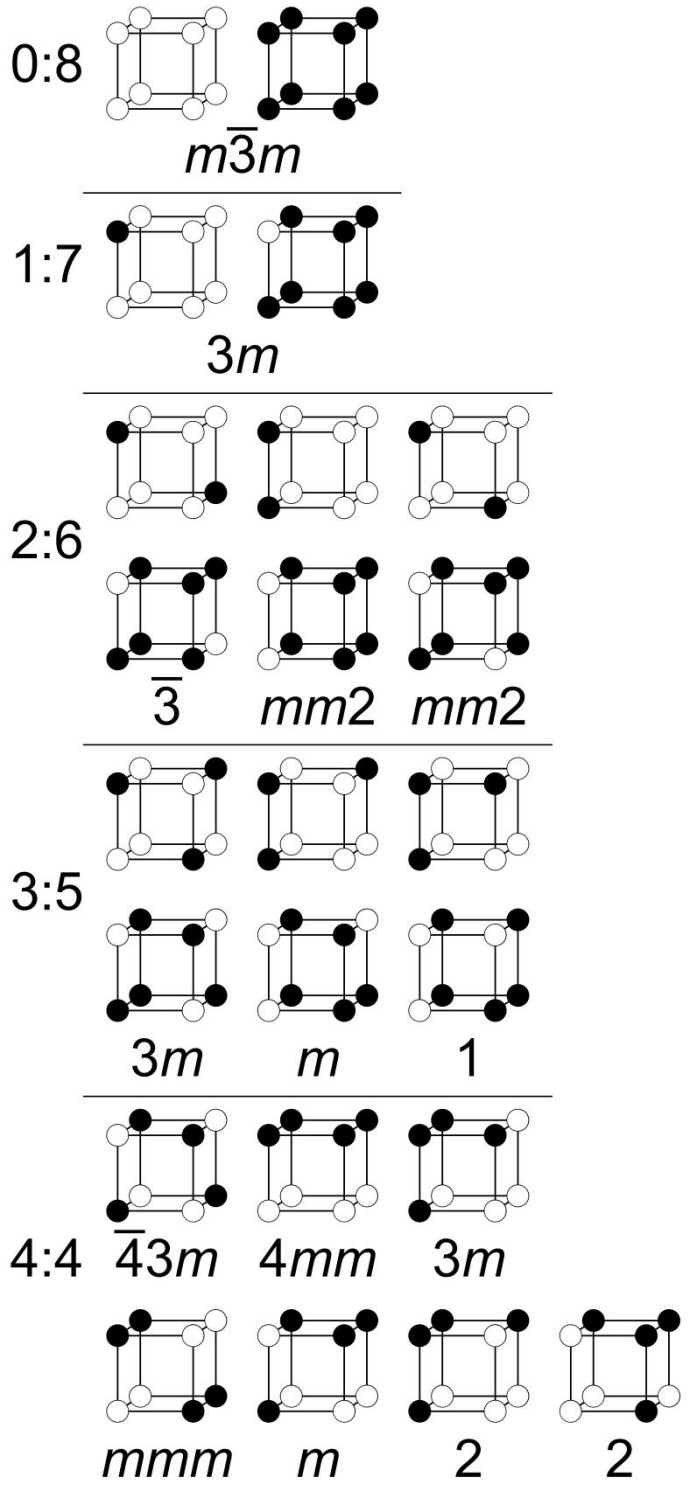

Figure S15 Ordering scheme for anions *X* and *Y* in fluorite type related compounds MX_xY_{2-x} ($0 < x < 2$) with 23 possible rotationally distinct two-coloring of eight vertices of a cube, derived from the Cauchy-Frobenius lemma (also called orbit-counting theorem, Burnside's lemma and even "the lemma that is not Burnside's")[8,9]. The respective point symmetries given below are often lowered in compounds MX_xY_{2-x} by distortion of the cubes.

Density Functional Theory (DFT) Calculations

Reaction Enthalpies

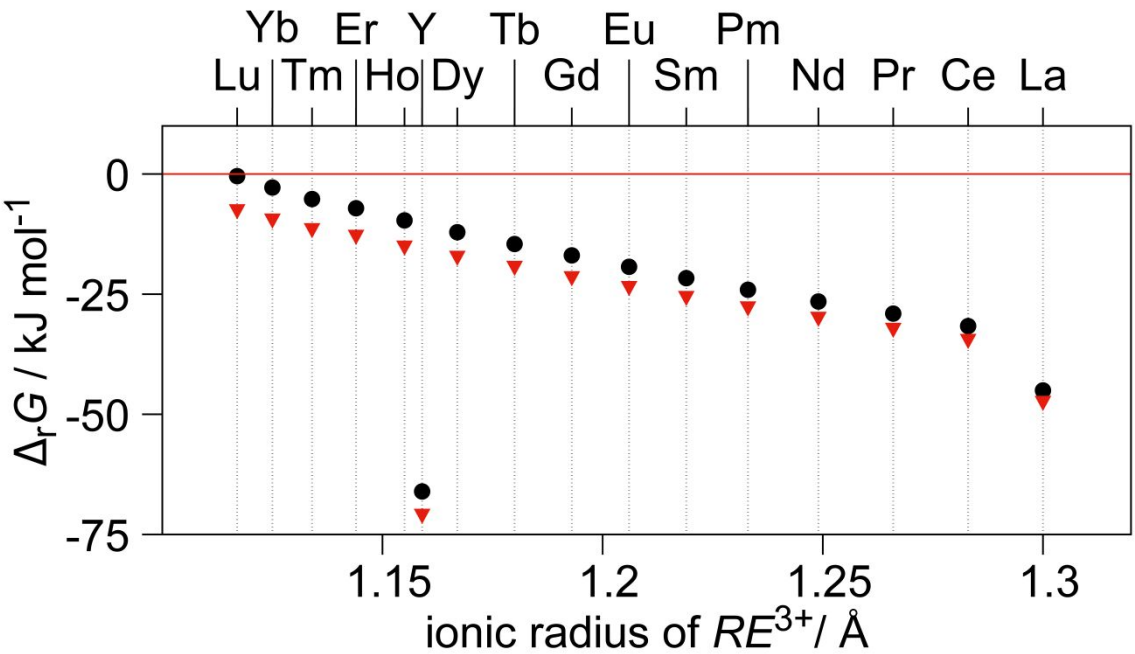

Figure S16 Reaction enthalpies derived from DFT calculations for the reaction RE_2O_3 + REH_3 = 3 *RE*HO for *RE*HO in LaHO type (black) and anit-LiMgN type (red) plotted against the ionic radii of the eight-fold coordinated trivalent *RE* ions.[3]

Density of States

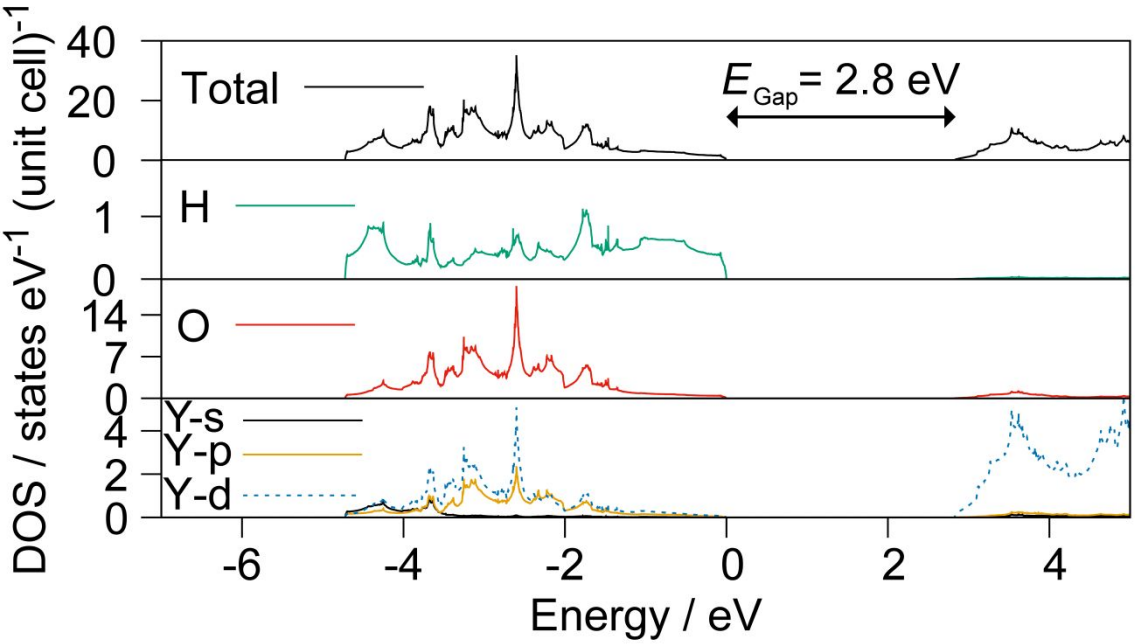

Figure S17 Total and projected density of states of YHO *Pnma*.

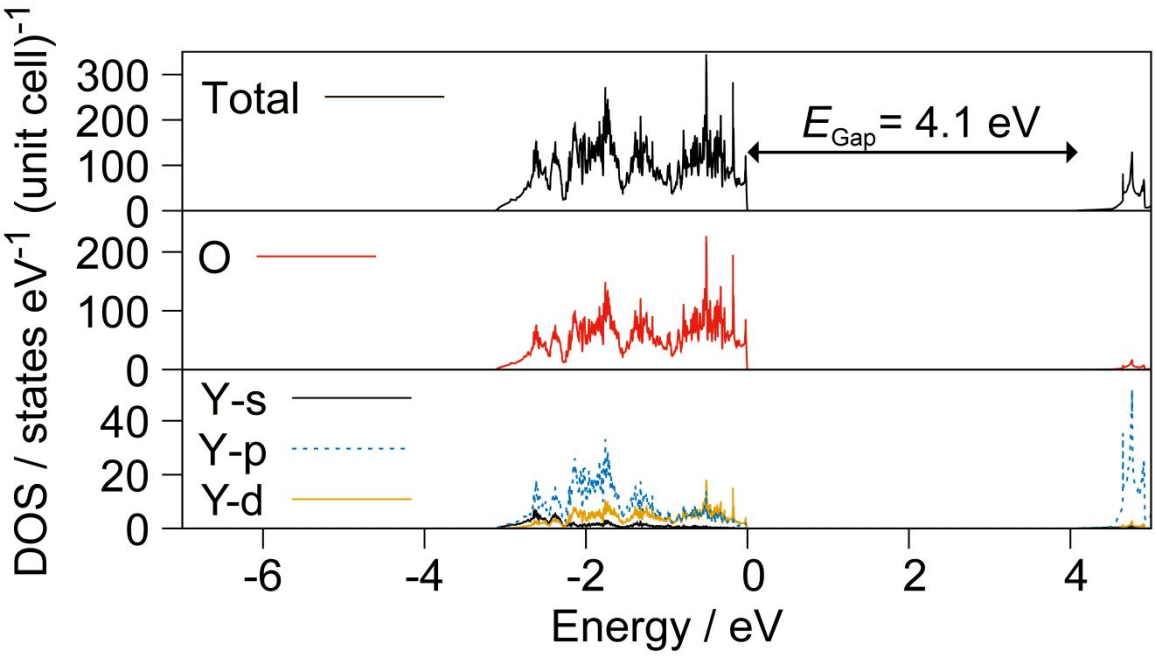

Figure S18 Total and projected density of states of Y_2O_3 $Ia\bar{3}$.

References

(1) J. Montero, F. A. Martinsen, M. García-Tecedor, S. Zh. Karazhanov, D. Maestre, B. Hauback, E. S. Marstein, Photochromic mechanism in oxygen-containing yttrium hydride thin films: An optical perspective, *Physical Review B* **2017**, *95*, 201301.

(2) A. Meyer, Symmetriebeziehungen zwischen Kristallstrukturen des Formeltyps AX_2, ABX_4, AB_2X_6 sowie deren Ordnungs- und Leerstellenvarianten, PhD thesis, University Karlsruhe, Karlsruhe, **1981**.

(3) R. D. Shannon, Revised Effective Ionic Radii and Systematic Studies of Interatomic Distances in Halides and Chalcogenides, *Acta Crystallographica* **1976**, *A 32*, 751-767.

(4) B. Malaman, J. F. Brice, Etude structurale de l'hydruro-oxyde LaHO par diffraction des rayons X et par diffraction de neutrons, *J. Solid State Chem.* **1984**, *53*, 44-54.

(5) J. F. Brice, A. Moreau, Synthese et cunductivite anionique des hy-druro-oxydes de lanthane de formule LaHO, $LaH_{1+2x}O_{1-x}$ et $LaH_{1+y}O_{1-x}$ (y<2x), *Ann. Chim. Fr.* **1982**, *7*, 623-634.

(6) M. Widerøe, H. Fjellvåg, T. Norby, F. W. Poulsen, R. W. Berg, NdHO, a novel oxyhydride, *J. Solid State Chem.* **2011**, *184*, 1890-1894.

(7) H. Yamashita, T. Broux, Y. Kobayashi, F. Takeiri, H. Ubukata, T. Zhu, M. A. Hayward, K. Fuji, M. Yashima, K. Shitara, A. Kuwabara, T. Murakami, H. Kageyama, Chemical Pressure-Induced Anion Order-Disorder Transition in LnHO Enabled by Hydride Size Flexibility, *J. Am. Chem. Soc.* **2018**, *140*, 11170-11173.

(8) P. M. Neumann, A lemma that is not Burnside's, *Math. Sci.* **1979**, *4*, 133–141.

(9) Md. Taufiq Nasseef, Counting Symmetries with Burnside's Lemma and Pólya's Theorem, *Eur. J. Pure Appl. Math.* **2016**, *9*, 84-113.